# Atomic density optimization of quasi-one-dimensional diffuse laser cooling under a two-dimensional magnetic-field gradient

Xiaolei Guan,[1] Mengyuan Han,[1] Jia Zhang,[1] Xun Gao,[1] Yu Wang,[2] Wei Zhuang,[3] Tiantian Shi,[4,5,*] and Jingbiao Chen[1,4,6,7,8]

[1]*Institute of Quantum Electronics, School of Electronics, Peking University, Beijing 100871, China*
[2]*National Key Laboratory for Metrology and Calibration Techniques, Changcheng Institute of Metrology & Measurement, Beijing 100095, China*
[3]*National Institute of Metrology, Beijing 100029, China*
[4]*National Key Laboratory of Advanced Micro and Nano Manufacture Technology, School of Integrated Circuits, Peking University, Beijing 100871, China*
[5]*Beijing Advanced Innovation Center for Integrated Circuits, Beijing 100871, China*
[6]*Hefei National Laboratory, Hefei 230088, China*
[7]*Handan Innovation Institute, Peking University, Handan 056107, China*
[8]*Beijing Key Laboratory of Quantum Metrology Technology and Instruments, Beijing 100871, China*

(Received 7 August 2026; accepted 21 October 2026; published 13 November 2026)

Diffuse laser cooling (DLC) provides a compact, robust, and scalable approach to generating cold-atom ensembles, offering significant potential for ground-based and spaceborne microwave atomic clocks. However, the performance of DLC systems remains limited by the weak atom-light interaction arising from their relatively low atomic density. This limitation is characterized by the optical density (OD), which quantifies the effective interaction strength between the atomic ensemble and the probe light and strongly influences the achievable signal-to-noise ratio. Although quasi-one-dimensional (quasi-1D) DLC extends the probe interaction length and improves atomic utilization, increasing the local atomic density within the interrogation region remains challenging. Here, we demonstrate a magnetically enhanced quasi-1D DLC system that simultaneously maintains the extended interaction length and increases the atomic density through a two-dimensional magnetic-field gradient. By spatially compressing and accumulating atoms near the probe axis, we enhance the OD of a 70-cm-long cold rubidium ensemble from 2.49 to 3.94, representing a 58% enhancement and an equivalent increase in the local atomic density. The dependence of the OD on the magnetic-field gradient, probe intensity, beam size, and cooling-light polarization is systematically investigated. This work establishes a practical pathway for enhancing optical interrogation efficiency and could pave the way for the development of high-performance DLC-based cold-atom clocks and quantum sensing systems.

DOI: 10.1103/8wmd-2s5q

## I. INTRODUCTION

Since the advent of the laser, advances in laser technology have enabled numerous breakthroughs in physics [1–3]. Among them, laser cooling and trapping of atoms [4–7] has undoubtedly emerged as one of the most rapidly developing and profoundly influential fields over the past few decades. This technology has not only fundamentally revolutionized our ability to manipulate atomic-scale motion and interactions, but also led to a series of major scientific achievements in precision measurement [8–11], quantum simulation [12,13], time and frequency standards [14–17], and even the exploration of novel states of matter [18], thereby serving as a crucial bridge between fundamental physics and cutting-edge applications. At the experimental level, several representative laser-cooling schemes have been established, including optical molasses [19], diffuse laser cooling (DLC) [20–22], and magneto-optical traps (MOTs) [23–25]. Each of these techniques possesses distinct characteristics and provides important tools for atomic manipulation and coherent control under different physical conditions.

Among the aforementioned laser-cooling schemes, DLC, a typical all-optical cooling technique, was first proposed theoretically by Yu-Zhu Wang in 1979 [20]. Its fundamental principle relies on the isotropic light field formed by photons scattered from diffuse reflective surfaces, which can effectively slow and cool atoms. In 1992, cooling of a sodium atomic beam using a diffuse light field was experimentally demonstrated for the first time [21]. Subsequently, this technique has been further developed in various high-reflectivity cavities, including copper [26,27], ceramic [22,28], silver-coated [29], and barium-sulfate-coated glass cavities [30,31].

*Contact author: tts@pku.edu.cn

*Published by the American Physical Society under the terms of the Creative Commons Attribution 4.0 International license. Further distribution of this work must maintain attribution to the author(s) and the published article's title, journal citation, and DOI.*

Compared with optical molasses and MOTs, DLC does not require precise alignment or collimation of laser beams, nor is it constrained by cavity geometry, resulting in a more compact, robust, and flexible system. Furthermore, atoms with different velocities can compensate for Doppler shifts by absorbing diffusely reflected light from different directions, thereby providing a larger capture velocity range and higher cooling efficiency. Its all-optical nature also eliminates the need for external magnetic fields, which is particularly advantageous for magnetically sensitive experiments. Owing to these features, DLC is widely regarded as an ideal approach for constructing simple and reliable cold-atom sources, especially for applications demanding high robustness and environmental adaptability, such as space cold-atom clocks [32,33] and portable atom interferometers [34].

It should be noted that a key challenge of DLC is its relatively low atomic density, typically on the order of $10^7\,\mathrm{cm}^{-3}$. This limitation arises from the inability of the diffuse light field to form a three-dimensional potential well that can efficiently accumulate atoms. Currently, several efforts have focused on optimizing the light-field configuration to increase the atomic density of DLC. For example, in integrating spheres or cylindrical cavities, the cold-atom density along the probe axis can be enhanced by adjusting the incidence angle [35], spatial position [36], and number of cooling beams, thereby improving the signal-to-noise ratio (SNR) of spectroscopic measurements. However, such approaches remain constrained by the geometry of conventional cavities, so only atoms within the volume traversed by the probe beam are effectively utilized, leaving the majority of cooled atoms unprobed. In 2022, a quasi-one-dimensional (quasi-1D) DLC scheme was proposed [37], in which cold atoms were prepared over a one-meter-long, horizontally oriented vacuum glass tube, achieving high spatial overlap between the probe beam and the cooling region. This design not only significantly extends the atom-light interaction length but also allows a much larger fraction of the cooled atoms to contribute to the measurement, offering a promising route for DLC applications in precision metrology [38,39] and space science [40].

In this work, we further explore the potential of the quasi-1D DLC scheme by introducing a two-dimensional magnetic-field gradient to enhance the atomic density. The magnetic field is generated by two pairs of orthogonally arranged anti-Helmholtz coils (AHCs), forming a potential well aligned with the probe axis, where the field is zero at the axis and increases gradually in the radial direction, thereby effectively compressing and accumulating cold atoms in its vicinity. Specifically, we use the optical density (OD), which is linearly proportional to the atomic density, as the key parameter for characterizing the system. We systematically investigate the effects of the magnetic-field gradient, probe intensity, beam size, and cooling-light polarization on the atomic density. Experimental results demonstrate that, under an optimal magnetic-field gradient of 6–7 G/cm, the OD of the 70-cm-long cold-atom ensemble increases from 2.49 to 3.94. As a further extension of quasi-1D DLC, this scheme preserves its inherent advantages, including long interaction length and high spatial utilization of atoms, while effectively increasing the number of probed atoms through magnetic confinement. In the future, this system could provide a promising route toward next-generation high-performance cold-atom clocks [29,41]. Under quantum-projection-noise-limited conditions, the SNR of the clock signal is proportional to $\sqrt{N}$, where $N$ is the number of atoms participating in the interrogation. Thus, increasing the number of probed atoms can enhance the clock-signal SNR and consequently improve the short-term frequency stability. Moreover, it holds considerable potential for applications in precision spectroscopy [42], quantum sensing, and high-precision quantum metrology [43,44].

## II. EXPERIMENTAL SETUP

Figure 1 illustrates the three-dimensional structure of the quasi-1D DLC system with two-dimensional magnetic-field gradient coils. The 780 nm cooling and repumping lasers are provided by two high-power tunable diode lasers (Toptica TA pro). We employ saturated absorption spectroscopy (SAS) to stabilize the cooling laser frequency to the $^{87}$Rb $5^2S_{1/2}\ F = 2 \rightarrow 5^2P_{3/2}\ F' = 3$ cycling transition, and the repumping laser frequency to the $F = 1 \rightarrow F' = 2$ transition. After stabilization, the cooling laser is red detuned by 15 MHz using acousto-optic modulators (AOMs). The cooling and repumping beams are then combined, split into four equal-power beams, and coupled into four multimode fibers. The total powers of the cooling and repumping lasers are approximately 165 and 40 mW, respectively. In contrast to conventional spherical or cylindrical DLC cavities, we use a 70-cm-long hollow glass tube with an inner diameter of 2 cm as the cooling chamber (vacuum level: $10^{-6}$ Pa). Its outer surface is coated with multiple layers of $BaSO_4$, providing high reflectivity over 250–1300 nm and exceeding 98% at 780 nm. Four small uncoated holes on the sidewall allow beam injection from the four fibers. Due to multiple diffuse reflections from the $BaSO_4$ coating, the injected beams form a quasi-1D diffuse light field with a relatively uniform intensity distribution inside the tube.

The two-dimensional magnetic-field gradient is generated by two pairs (four in total) of orthogonally arranged AHCs, each coil measuring 80 cm × 20 cm and wound with 200 turns of copper wire. Each pair is driven by an independent current supply, with current directions indicated in the lower-left corner of Fig. 1(b). By adjusting the currents, the magnetic-field gradients along the $x$ and $y$ directions can be independently controlled. Figures 1(c)–1(e) show the measured one-dimensional magnetic-field distributions along each axis, obtained using a magnetometer with 0.1 G resolution. The coordinate origin is defined at the geometric center of the coil assembly. A zero-field line is observed along the longitudinal ($z$) direction. At any point on this line, the magnetic-field intensities along $x$ and $y$ vary linearly with displacement from the center, with opposite directions on either side. To quantify the gradient characteristics, we record the gradients along the $x$ and $y$ directions under different driving currents. Since the two pairs of AHCs have identical structures, the measured gradients are both 2.9 G/(cm A). This two-dimensional magnetic-field gradient, together with the diffuse light field, forms a magneto-optical potential well, which drives atoms uniformly distributed within the glass

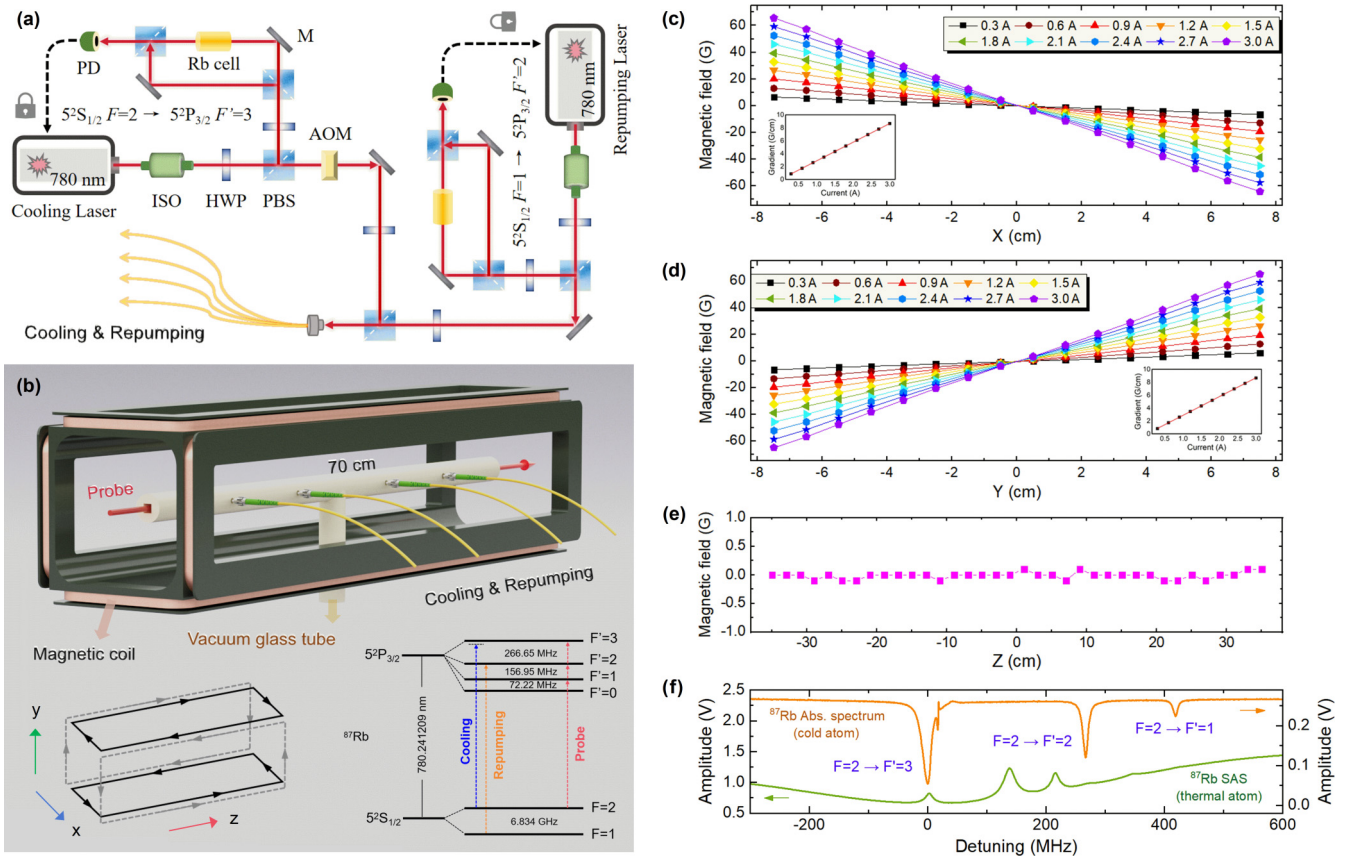



FIG. 1. (a) Optical setup of the cooling and repumping lasers. ISO: isolator; HWP: half-wave plate; PBS: polarizing beam splitter; M: high-reflection mirror; PD: photodetector; AOM: acousto-optic modulator. (b) Conceptual sketch of the quasi-1D DLC system with two-dimensional magnetic-field gradient coils. The vacuum glass tube is 70 cm long with an inner diameter of 2 cm. Two pairs of orthogonally arranged anti-Helmholtz coils consist of four independent coils (80 cm × 20 cm, 200 turns each), with current directions shown in the lower-left corner. The probe laser propagates along the $z$ axis. (c), (d) Magnetic-field distributions along the $x$ and $y$ axes under different driving currents. The magnetic-field gradient is 2.9 G/(cm A) for both axes. (e) Magnetic-field distribution along the central axis ($z$ direction) of the coil assembly, remaining approximately zero over the entire 70 cm length. (f) Absorption spectrum of cold $^{87}$Rb atoms (orange). The green curve shows the SAS reference obtained from thermal atoms.

tube toward the zero-field line, thereby increasing the atomic density in its vicinity.

Next, we precisely align the zero-field line with the central axis of the glass tube and use a 780 nm external-cavity diode laser as the probe source, with the probe beam propagating along the tube axis to measure the absorption spectrum of the cold atoms. The probe laser frequency is continuously scanned across the $^{87}$Rb $5^2S_{1/2}$ $F = 2 \rightarrow 5^2P_{3/2}$ transition. Taking the thermal-atom SAS as a reference, the three absorption peaks in the orange curve of Fig. 1(f) correspond, from left to right, to the $F = 2 \rightarrow F' = 3$, 2, 1 hyperfine transitions. To more intuitively evaluate the cold-atom density enhancement, we use the OD, which is linearly proportional to the atomic density $\rho$, as the key characterization parameter. It is calculated from the absorption spectra according to $\mathrm{OD} = -\ln \frac{I_{\mathrm{out}}}{I_{\mathrm{in}}} = \rho\sigma(\delta)L$, where $I_{\mathrm{in}}$ and $I_{\mathrm{out}}$ are the incident and transmitted probe intensities, respectively, $\sigma(\delta) = \frac{3\lambda^2}{2\pi}\frac{1}{1+4(\delta/\Gamma)^2}$ is the effective absorption cross section of the atoms (with $\lambda$ the laser wavelength, $\delta$ the detuning of the probe laser frequency from the atomic resonance, and $\Gamma$ the natural linewidth of the transition), and $L$ is the interaction length between the probe beam and the atomic ensemble. When the probe laser is on resonance, the cold-atom density can be derived as $\rho = \mathrm{OD} \times \frac{2\pi}{3\lambda^2 L}$. In the following experiments, all OD measurements are performed on the $F = 2 \rightarrow F' = 3$ cycling transition.

## III. RESULTS

### A. Optimization of the magnetic-field gradient

The two-dimensional magnetic-field gradient is a key parameter for controlling the density of cold atoms. To clarify its influence, we independently vary the driving currents of the two pairs of AHCs and measure the OD under different gradient configurations. Figures 2(a)–2(c) show the results for probe intensities of 0.75, 1.5, and 3 mW/cm$^2$. In the absence of applied gradient fields, the initial ODs are 2.49, 1.82, and 1.16, corresponding to atomic densities of $1.22 \times 10^7$, $8.95 \times 10^6$, and $5.71 \times 10^6$ cm$^{-3}$, respectively. Scanning the magnetic-field gradients in both $x$ and $y$ directions over the range of 1–9 G/cm reveals a consistent trend for all three probe intensities: When the gradients are relatively weak (<5 G/cm) or imbalanced between the two directions, the OD enhancement is limited; when both gradients exceed 5 G/cm

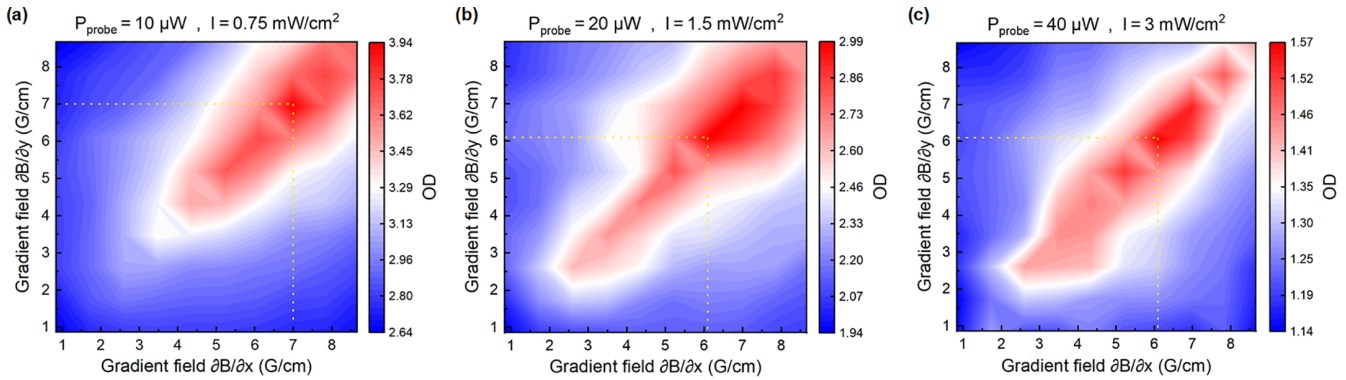



FIG. 2. OD measurements under different two-dimensional magnetic-field gradients. The probe intensities are (a) 0.75, (b) 1.5, and (c) 3 $mW/cm^2$, with initial ODs of 2.49, 1.82, and 1.16 in the absence of applied gradient fields. The probe beam has a Gaussian diameter of 1.3 mm in all cases.

and are approximately equal, the OD increases significantly. The optimal gradient range lies around 6–7 G/cm, yielding maximum ODs of 3.94, 2.99, and 1.57, which correspond to atomic densities of $1.94 \times 10^7$, $1.47 \times 10^7$, and $7.72 \times 10^6$ $cm^{-3}$, respectively.

### B. Analysis of density characteristics

With the magnetic-field gradients along the $x$ and $y$ directions fixed at the optimal value of 6.5 G/cm, we next expand the probe beam and measure the OD as a function of probe power for expansion factors of 1 (unexpanded), 2, 3, 4, and 5. The insets in Figs. 3(a)–3(e) show the corresponding probe-beam profiles measured using a beam quality analyzer (Thorlabs BP209), with Gaussian diameters of 1.3, 2.8, 3.9, 4.8, and 5.7 mm, respectively. In each subfigure, the OD exhibits a similar dependence on probe power both with (red) and without (blue) the magnetic-field gradient. When the probe beam is unexpanded, the OD decreases rapidly with increasing probe power because the probe intensity far exceeds the saturation intensity at 780 nm ($I_{sat} \approx 1.67\,mW/cm^2$), causing heating, expansion, and displacement of the cold-atom cloud and thereby reducing the number of atoms probed. With an expansion factor of 2, the decline in OD slows markedly, while for expansion factors of 3, 4, and 5, the OD remains nearly constant as the probe power increases because the probe intensity is well below $I_{sat}$. These results indicate that the incident light intensity is a key factor affecting the cold-atom density. For applications requiring high atomic density, expanding the incident beam is therefore beneficial for maintaining the stability of the cold-atom cloud.

Furthermore, Fig. 3 reveals another important feature of the cold-atom density distribution in the two-dimensional magnetic-field gradient configuration. Although expanding the probe beam by factors of 3, 4, and 5 suppresses the OD decrease with increasing power, the OD enhancement provided by the gradient field gradually diminishes as the beam diameter increases. This behavior arises because the cold-atom cloud exhibits high density only near the zero-field line. As the radial magnetic field strength increases, the atomic density decreases due to reduced cooling efficiency from the Zeeman effect and enhanced atom loss induced by collisions. Consequently, for the same probe intensity, an excessively large probe beam fails to efficiently utilize the high-density atoms concentrated along the central zero-field line, resulting in a loss of the OD enhancement factor. Overall, under the condition that the cold-atom density remains stable with increasing incident laser power, a threefold expansion of the incident beam is the optimal choice for subsequent applications.

### C. Comparison of different cooling-beam polarization configurations

All experiments described above are performed under the conventional DLC configuration, where no active polarization control is applied to the incident cooling and repumping beams. After transmission through multimode fibers, the initially linearly polarized light becomes depolarized. Following multiple diffuse reflections inside the glass tube, the scattered light superposes to form an approximately isotropic and unpolarized optical field. To investigate the effect of polarization on DLC performance, we replace the incident cooling and repumping beams with circularly polarized light. The experimental setup is shown in Fig. 4(a). Eight linearly polarized cooling and repumping beams are delivered through eight polarization-maintaining single-mode fibers and then pass through a half-wave plate, a polarizing beam splitter, and a quarter-wave plate, generating four pairs of counterpropagating $\sigma^+$ and $\sigma^-$ circularly polarized beams. These beams are injected into the vacuum chamber through apertures on opposite sides of the glass tube. Following the conventional DLC optimization procedure [17,37], we first measure the OD as a function of the cooling and repumping laser powers [Figs. 4(b) and 4(c)]. The OD reaches its maximum when the total power of the circularly polarized cooling beams is approximately 180 mW and that of the repumping beams is approximately 20 mW. Note that the maximum available cooling-laser power is limited to 180 mW due to the coupling efficiency of the polarization-maintaining fibers.

Then, with the cooling and repumping laser powers fixed at the optimal values mentioned above, we apply the two-dimensional magnetic-field gradient to the DLC in the circularly polarized configuration and measure the OD for different gradient settings (probe power: 10 μW, unexpanded). In the absence of a magnetic-field gradient, the initial OD

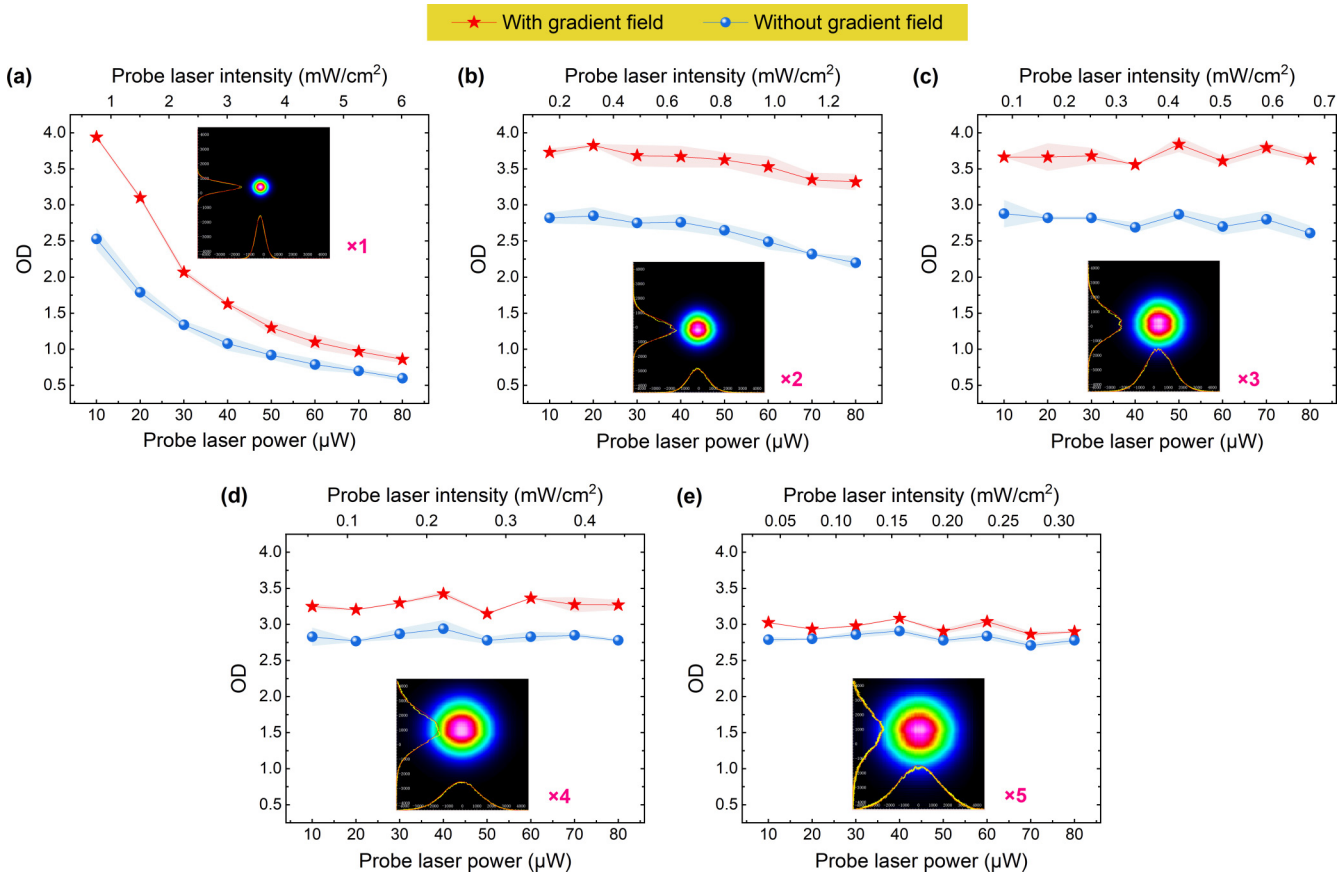



FIG. 3. OD as a function of probe laser power (intensity) for different probe-beam sizes. The red and blue curves represent measurements with and without the two-dimensional magnetic-field gradient, respectively. Each data point is the average of three measurements. From panel (a) to panel (e), the probe beam expansion factors are 1 (unexpanded), 2, 3, 4, and 5, with corresponding Gaussian diameters of 1.3, 2.8, 3.9, 4.8, and 5.7 mm.

of the cold-atom cloud reaches 3, exceeding the value of 2.49 obtained without polarization control. We attribute this improvement to the fact that the circularly polarized incident beams, after diffuse reflection, form a partially coherent optical field with a complex polarization structure, which generates numerous small and steep "polarization gradients" [45]. As atoms move through this field, they repeatedly undergo Sisyphus cooling cycles, resulting in higher cooling efficiency. Additionally, as shown in Fig. 4(d), the OD increases slightly only when the gradient strength is smaller than 4 G/cm. This is because the gradient field exerts a magnetic force on moving atoms, pulling them toward regions of lower field strength. However, when the gradient is too large, the polarization-gradient-based cooling mechanism is disrupted, leading to an OD lower than that without the magnetic field.

Finally, Fig. 4(e) compares the OD as a function of probe laser power for the conventional configuration without polarization control and the circularly polarized configuration, each operated at its optimal magnetic-field gradient (6.5 and 3 G/cm, respectively). The results show that the OD obtained with the circularly polarized configuration (blue) is consistently lower than that in the conventional configuration (red). We speculate that this difference arises from the optical field inside the circularly polarized DLC exhibiting a more complex polarization structure, which may generate a repulsive force that pushes atoms away from the zero-field line, thereby weakening the effectiveness of magnetic confinement. Therefore, the two-dimensional magnetic-field gradient is more suitable for the conventional DLC system without active polarization control.

## IV. CONCLUSION

In this work, we demonstrate a magnetic-field-engineered quasi-1D DLC system that enables an increase in atomic density while preserving the extended interaction length characteristic of the quasi-1D configuration. By introducing a two-dimensional magnetic-field gradient, we spatially compress and accumulate cold atoms near the probe axis, thereby strengthening the atom-light interaction. Through systematic investigation of the effects of the magnetic-field gradient, probe parameters, and cooling-light polarization, the optimal operating conditions are identified, enabling a 58% increase in the OD (from 2.49 to 3.94) and an equivalent increase in the local atomic density of the 70-cm-long cold rubidium ensemble.

This approach combines the advantages of long interaction length and enhanced atomic utilization. It could be applied to cold-atom active Faraday optical frequency standards [46], where the increased atomic density may improve the transmission of cold-atom Faraday filters [47–49], thereby facilitating stimulated emission and enabling further narrowing

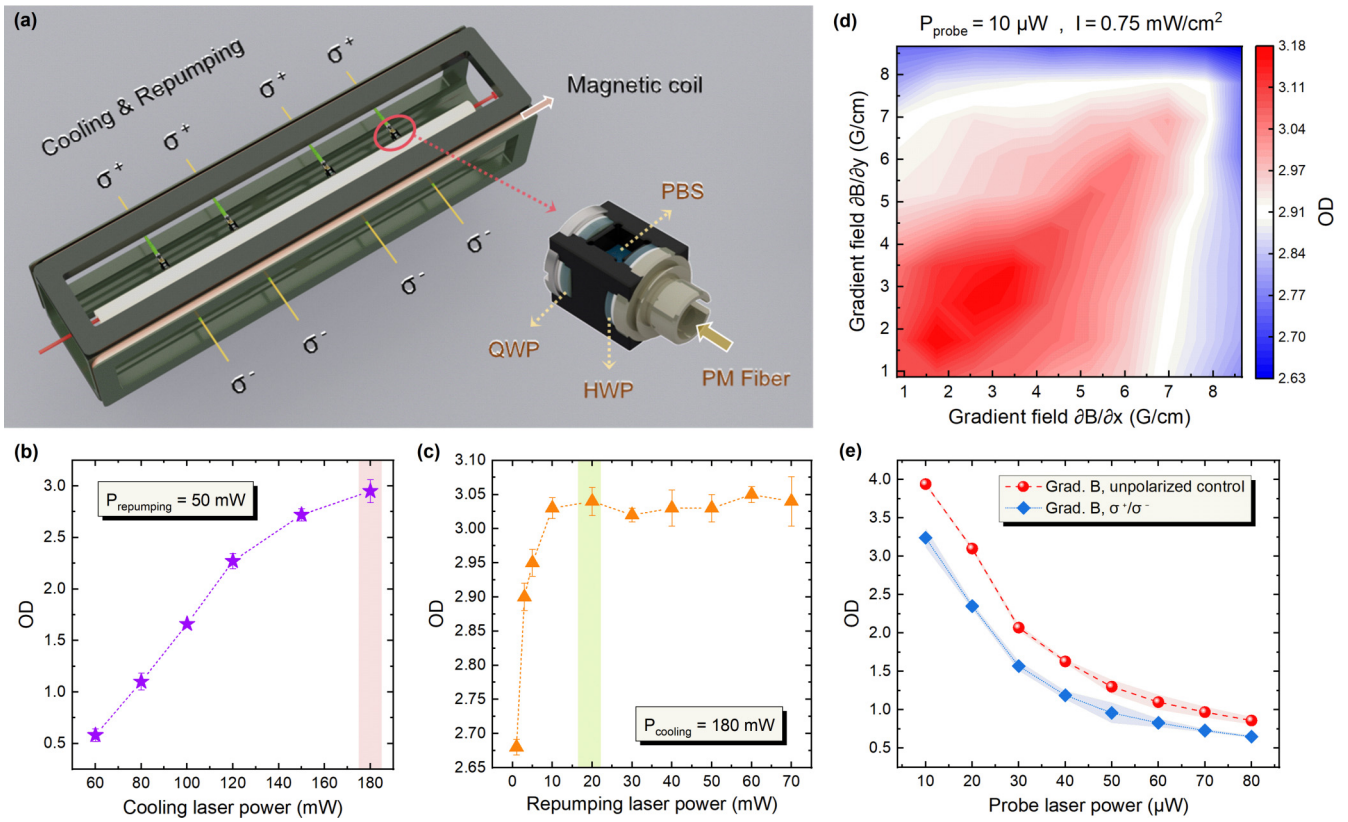



FIG. 4. Experimental results of the quasi-1D DLC system using circularly polarized cooling and repumping lasers. (a) Schematic of the experimental setup. PM: polarization-maintaining; HWP: half-wave plate; PBS: polarizing beam splitter; QWP: quarter-wave plate. (b) OD vs cooling laser power with repumping power fixed at 50 mW. (c) OD vs repumping laser power with cooling power fixed at 180 mW. (d) OD measurements under different two-dimensional magnetic-field gradients. The probe intensity is $0.75\,\mathrm{mW/cm^2}$ and the initial OD without the gradient field is 3. (e) Comparison of OD between conventional DLC (without polarization control, red) and the circularly polarized configuration (blue) at their respective optimal magnetic-field gradients. Each data point in panels (b), (c), and (e) is the average of three measurements.

of the laser linewidth. For cold-atom clocks [29,40,41], under quantum-projection-noise-limited conditions and assuming that the effective number of interrogated atoms increases correspondingly, the 58% increase in atom number could yield an SNR enhancement of approximately 26% ($\sqrt{1.58} \approx 1.26$), thereby potentially improving short-term frequency stability. More broadly, this approach establishes a pathway toward compact, high-performance cold-atom frequency standards [17] and precision quantum sensors [50,51].

## ACKNOWLEDGMENTS

This research was funded by the Quantum Science and Technology—National Science and Technology Major Project (2021ZD0303200), National Natural Science Foundation of China (62405007), JSJL2024205XXXX, and Hebei Provincial Natural Science Foundation Basic Research Special Project—2025 Basic Research Program Proof-of-Concept Project (F2025109009).

J.C. conceived the idea of enhancing the atomic density in quasi-one-dimensional diffuse laser cooling by employing a two-dimensional magnetic-field gradient. X.G. performed the experiments and wrote the manuscript. M.H., J.Z., X.G., Y.W., W.Z., and T.S. participated in the discussion of results and revision of the manuscript.

The authors declare no competing interests.

## DATA AVAILABILITY

The data that supports the plots within this paper and other findings of this study are available from the corresponding authors upon reasonable request.

[1] M. H. Anderson, J. R. Ensher, M. R. Matthews, C. E. Wieman, and E. A. Cornell, Observation of Bose-Einstein condensation in a dilute atomic vapor, Science **269**, 198 (1995).

[2] M. Kourogi, K. Nakagawa, and M. Ohtsu, Wide-span optical frequency comb generator for accurate optical frequency difference measurement, IEEE J. Quantum Electron. **29**, 2693 (2002).

[3] P. M. Paul, E. S. Toma, P. Breger, G. Mullot, F. Augé, P. Balcou, H. G. Muller, and P. Agostini, Observation of a train of attosecond pulses from high harmonic generation, Science **292**, 1689 (2001).

[4] A. Ashkin, Acceleration and trapping of particles by radiation pressure, Phys. Rev. Lett. **24**, 156 (1970).

[5] T. W. Hänsch and A. L. Schawlow, Cooling of gases by laser radiation, Opt. Commun. **13**, 68 (1975).

[6] W. D. Phillips and H. Metcalf, Laser deceleration of an atomic beam, Phys. Rev. Lett. **48**, 596 (1982).

[7] P. D. Lett, R. N. Watts, C. I. Westbrook, W. D. Phillips, P. L. Gould, and H. J. Metcalf, Observation of atoms laser cooled below the Doppler limit, Phys. Rev. Lett. **61**, 169 (1988).

[8] M. Kasevich and S. Chu, Atomic interferometry using stimulated Raman transitions, Phys. Rev. Lett. **67**, 181 (1991).

[9] M. Takamoto, I. Ushijima, N. Ohmae, T. Yahagi, K. Kokado, H. Shinkai, and H. Katori, Test of general relativity by a pair of transportable optical lattice clocks, Nat. Photon. **14**, 411 (2020).

[10] P. Cladé, E. de Mirandes, M. Cadoret, S. Guellati-Khélifa, C. Schwob, F. Nez, L. Julien, and F. Biraben, Determination of the fine structure constant based on Bloch oscillations of ultracold atoms in a vertical optical lattice, Phys. Rev. Lett. **96**, 033001 (2006).

[11] J. J. Hudson, D. M. Kara, I. Smallman, B. E. Sauer, M. R. Tarbutt, and E. A. Hinds, Improved measurement of the shape of the electron, Nature (London) **473**, 493 (2011).

[12] J. Argüello-Luengo, A. González-Tudela, T. Shi, P. Zoller, and J. I. Cirac, Quantum simulation of two-dimensional quantum chemistry in optical lattices, Phys. Rev. Res. **2**, 042013(R) (2020).

[13] H.-J. Shao, Y.-X. Wang, D.-Z. Zhu, Y.-S. Zhu, H.-N. Sun, S.-Y. Chen, C. Zhang, Z.-J. Fan, Y. Deng, X.-C. Yao, Y.-A. Chen, and J.-W. Pan, Antiferromagnetic phase transition in a 3D fermionic Hubbard model, Nature (London) **632**, 267 (2024).

[14] A. Aeppli, K. Kim, W. Warfield, M. S. Safronova, and J. Ye, Clock with $8 \times 10^{-19}$ systematic uncertainty, Phys. Rev. Lett. **133**, 023401 (2024).

[15] Y. Huang, B. Zhang, M. Zeng, Y. Hao, Z. Ma, H. Zhang, H. Guan, Z. Chen, M. Wang, and K. Gao, Liquid-nitrogen-cooled $Ca^+$ optical clock with systematic uncertainty of $3 \times 10^{-18}$, Phys. Rev. Appl. **17**, 034041 (2022).

[16] S. L. Campbell, R. B. Hutson, G. E. Marti, A. Goban, N. D. Oppong, R. L. McNally, L. Sonderhouse, J. M. Robinson, W. Zhang, B. J. Bloom, and J. Ye, A Fermi-degenerate three-dimensional optical lattice clock, Science **358**, 90 (2017).

[17] X. Guan, J. Zhang, X. Gao, Y. Wang, T. Shi, and J. Chen, A 780 nm optical frequency standard based on diffuse laser cooled $^{87}$Rb atoms, Appl. Phys. Lett. **126**, 031104 (2025).

[18] P. Wcisło, P. Morzyński, M. Bober, A. Cygan, D. Lisak, R. Ciuryło, and M. Zawada, Experimental constraint on dark matter detection with optical atomic clocks, Nat. Astron. **1**, 0009 (2016).

[19] S. Chu, L. Hollberg, J. E. Bjorkholm, A. Cable, and A. Ashkin, Three-dimensional viscous confinement and cooling of atoms by resonance radiation pressure, Phys. Rev. Lett. **55**, 48 (1985).

[20] Y. Wang, Atomic beam slowing by diffuse light in an integrating sphere, in *Proceedings of the National Symposium on Frequency Standards, Chengdu, China* (1979) (unpublished).

[21] W. Ketterle, A. Martin, M. A. Joffe, and D. E. Pritchard, Slowing and cooling atoms in isotropic laser light, Phys. Rev. Lett. **69**, 2483 (1992).

[22] H.-D. Cheng, W.-Z. Zhang, H.-Y. Ma, L. Liu, and Y.-Z. Wang, Laser cooling of rubidium atoms from background vapor in diffuse light, Phys. Rev. A **79**, 023407 (2009).

[23] E. L. Raab, M. Prentiss, A. Cable, S. Chu, and D. E. Pritchard, Trapping of neutral sodium atoms with radiation pressure, Phys. Rev. Lett. **59**, 2631 (1987).

[24] C. Monroe, W. Swann, H. Robinson, and C. Wieman, Very cold trapped atoms in a vapor cell, Phys. Rev. Lett. **65**, 1571 (1990).

[25] A. Takamizawa, R. Hokari, S. Kagami, T. H. H. Le, K. Matsumoto, R. Takei, K. Hagimoto, and S. Yanagimachi, Magneto-optical trap with a hollow grating and an additional retroreflected laser beam, Appl. Phys. Lett. **126**, 244006 (2025).

[26] E. Guillot, P.-E. Pottie, and N. Dimarcq, Three-dimensional cooling of cesium atoms in a reflecting copper cylinder, Opt. Lett. **26**, 1639 (2001).

[27] X.-C. Wang, H.-D. Cheng, L. Xiao, B.-C. Zheng, Y.-L. Meng, L. Liu, and Y.-Z. Wang, Measurement of spatial distribution of cold atoms in an integrating sphere, Chin. Phys. Lett. **29**, 023701 (2012).

[28] W.-Z. Zhang, H.-D. Cheng, L. Liu, and Y.-Z. Wang, Observation of recoil-induced resonances and electromagnetically induced absorption of diffuse light by cold atoms, Phys. Rev. A **79**, 053804 (2009).

[29] P. Liu, Y. Meng, J. Wan, X. Wang, Y. Wang, L. Xiao, H. Cheng, and L. Liu, Scheme for a compact cold-atom clock based on diffuse laser cooling in a cylindrical cavity, Phys. Rev. A **92**, 062101 (2015).

[30] X. Wang, Y. Sun, and L. Liu, Characterization of isotropic laser cooling for application in quantum sensing, Opt. Express **29**, 43435 (2021).

[31] X. Wang, Y. Sun, H.-D. Cheng, J.-Y. Wan, Y.-L. Meng, L. Xiao, and L. Liu, Nearly nondestructive thermometry of labeled cold atoms and application to isotropic laser cooling, Phys. Rev. Appl. **14**, 024030 (2020).

[32] Y.-L. Meng, X.-J. Jiang, J. Wu, M.-F. Ye, H.-D. Cheng, L. Li, and L. Liu, Satellite-borne atomic clock based on diffuse laser-cooled atoms, Front. Phys. **10**, 985586 (2022).

[33] M. Langlois, L. De Sarlo, D. Holleville, N. Dimarcq, J.-F. Schaff, and S. Bernon, Compact cold-atom clock for onboard timebase: Tests in reduced gravity, Phys. Rev. Appl. **10**, 064007 (2018).

[34] C. LeDesma, K. Mehling, J. Shao, J. D. Wilson, P. Axelrad, M. Nicotra, D. Z. Anderson, and M. Holland, Demonstration of a programmable optical lattice atom interferometer, Phys. Rev. Res. **6**, 043120 (2024).

[35] Y.-L. Meng, H.-D. Cheng, P. Liu, B.-C Zheng, L. Xiao, J. Wan, X.-M. Wang, and L. Liu, Increasing the cold atom density in an integrating spherical cavity, Phys. Lett. A **378**, 2034 (2014).

[36] Y.-L. Meng, H.-D. Cheng, B.-C. Zheng, X.-C. Wang, L. Xiao, and L. Liu, Controlling the shape of a cold atom cloud in a cylindrical cavity, Chin. Phys. Lett. **30**, 063701 (2013).

[37] J.-Y. Wan, X. Wang, X. Zhang, Y.-L. Meng, W.-L. Wang, Y. Sun, and L. Liu, Quasi-one-dimensional diffuse laser cooling of atoms, Phys. Rev. A **105**, 033110 (2022).

[38] Y. Cohen, K. Jadeja, S. Sula, M. Venturelli, C. Deans, L. Marmugi, and F. Renzoni, A cold atom radio-frequency magnetometer, Appl. Phys. Lett. **114**, 073505 (2019).

[39] Y. Wang, Y. Meng, J. Wan, L. Xiao, M. Yu, X. Wang, X. Ouyang, H. Cheng, and L. Liu, Reaching a few $10^{-15}$ long-term stability of integrating sphere cold atom clock, Chin. Opt. Lett. **16**, 070201 (2018).

[40] L. Liu, D.-S. Lü, W.-B. Chen, T. Li, Q.-Z. Qu, B. Wang, L. Li, W. Ren, Z.-R. Dong, J.-B. Zhao, *et al.*, In-orbit operation of an atomic clock based on laser-cooled $^{87}$Rb atoms, Nat. Commun. **9**, 2760 (2018).

[41] F.-X. Esnault, D. Holleville, N. Rossetto, S. Guerandel, and N. Dimarcq, High-stability compact atomic clock based on isotropic laser cooling, Phys. Rev. A **82**, 033436 (2010).

[42] C. Han, B. Lu, and C. Lee, Ramsey interferometry with cold atoms in coherent population trapping, Adv. Phys.: X **9**, 2317896 (2024).

[43] J. Grotti, S. Koller, S. Vogt, S. Häfner, U. Sterr, C. Lisdat, H. Denker, C. Voigt, L. Timmen, A. Rolland, *et al.*, Geodesy and metrology with a transportable optical clock, Nat. Phys. **14**, 437 (2018).

[44] S. Kolkowitz, I. Pikovski, N. Langellier, M. D. Lukin, R. L. Walsworth, and J. Ye, Gravitational wave detection with optical lattice atomic clocks, Phys. Rev. D. **94**, 124043 (2016).

[45] J. Dalibard and C. Cohen-Tannoudji, Laser cooling below the Doppler limit by polarization gradients: Simple theoretical models, J. Opt. Soc. Am. B. **6**, 2023 (1989).

[46] W. Zhuang and J. Chen, Active Faraday optical frequency standard, Opt. Lett. **39**, 6339 (2014).

[47] W. Zhuang, Y. Zhao, S. Wang, Z. Fang, F. Fang, and T. Li, Ultranarrow bandwidth Faraday atomic filter approaching natural linewidth based on cold atoms, Chin. Opt. Lett. **19**, 030201 (2021).

[48] X. Guan, W. Zhuang, T. Shi, J. Miao, J. Zhang, J. Chen, and B. Luo, 420-nm Faraday optical filter with 2.7-MHz ultranarrow bandwidth based on laser cooled $^{87}$Rb atoms, IEEE Photon. Technol. Lett. **35**, 672 (2023).

[49] X. Guan, W. Zhuang, T. Shi, J. Miao, J. Zhang, J. Chen, and B. Luo, Cold-atom optical filtering enhanced by optical pumping, Front. Phys. **10**, 1090483 (2022).

[50] C.-W. Chou, D. B. Hume, T. Rosenband, and D. J. Wineland, Optical clocks and relativity, Science **329**, 1630 (2010).

[51] A. Hees, J. Guéna, M. Abgrall, S. Bize, and P. Wolf, Searching for an oscillating massive scalar field as a dark matter candidate using atomic hyperfine frequency comparisons, Phys. Rev. Lett. **117**, 061301 (2016).